

GLGait: A Global-Local Temporal Receptive Field Network for Gait Recognition in the Wild

Guozhen Peng
State Key Laboratory of Virtual
Reality Technology and Systems,
Beihang University
guozhen_peng@buaa.edu.cn

Yunhong Wang
State Key Laboratory of Virtual
Reality Technology and Systems,
Beihang University
yhwang@buaa.edu.cn

Yuwei Zhao
State Key Laboratory of Virtual
Reality Technology and Systems,
Beihang University
sy2206328@buaa.edu.cn

Shaoxiong Zhang
The School of Communication
Engineering, Hangzhou Dianzi
University
zhangsx@hdu.edu.cn

Annan Li*
State Key Laboratory of Virtual
Reality Technology and Systems,
Beihang University
liannan@buaa.edu.cn

Abstract

Gait recognition has attracted increasing attention from academia and industry as a human recognition technology from a distance in non-intrusive ways without requiring cooperation. Although advanced methods have achieved impressive success in lab scenarios, most of them perform poorly in the wild. Recently, some Convolution Neural Networks (ConvNets) based methods have been proposed to address the issue of gait recognition in the wild. However, the temporal receptive field obtained by convolution operations is limited for long gait sequences. If directly replacing convolution blocks with visual transformer blocks, the model may not enhance a local temporal receptive field, which is important for covering a complete gait cycle. To address this issue, we design a Global-Local Temporal Receptive Field Network (GLGait). GLGait employs a Global-Local Temporal Module (GLTM) to establish a global-local temporal receptive field, which mainly consists of a Pseudo Global Temporal Self-Attention (PGTA) and a temporal convolution operation. Specifically, PGTA is used to obtain a pseudo global temporal receptive field with less memory and computation complexity compared with a multi-head self-attention (MHSA). The temporal convolution operation is used to enhance the local temporal receptive field. Besides, it can also aggregate pseudo global temporal receptive field to a true holistic temporal receptive field. Furthermore, we also propose a Center-Augmented Triplet Loss (CTL) in GLGait to reduce the intra-class distance and expand the positive samples in the training stage. Extensive experiments show that our method obtains state-of-the-art results on in-the-wild datasets, *i.e.*, Gait3D and GREW. The code is available at <https://github.com/bgdpgz/GLGait>.

*Corresponding author.

Permission to make digital or hard copies of all or part of this work for personal or classroom use is granted without fee provided that copies are not made or distributed for profit or commercial advantage and that copies bear this notice and the full citation on the first page. Copyrights for components of this work owned by others than the author(s) must be honored. Abstracting with credit is permitted. To copy otherwise, or republish, to post on servers or to redistribute to lists, requires prior specific permission and/or a fee. Request permissions from permissions@acm.org.

MM '24, October 28–November 1, 2024, Melbourne, VIC, Australia.

© 2024 Copyright held by the owner/author(s). Publication rights licensed to ACM.

ACM ISBN 979-8-4007-0686-8/24/10

<https://doi.org/10.1145/3664647.3680812>

CCS Concepts

• Computing methodologies → Biometrics.

Keywords

Gait Recognition, In the Wild, Global-Local Temporal Receptive Field, Gait Silhouette Sequence, Neural Network

ACM Reference Format:

Guozhen Peng, Yunhong Wang, Yuwei Zhao, Shaoxiong Zhang, and Annan Li. 2024. GLGait: A Global-Local Temporal Receptive Field Network for Gait Recognition in the Wild. In *Proceedings of the 32nd ACM International Conference on Multimedia (MM '24)*, October 28–November 1, 2024, Melbourne, VIC, Australia. ACM, New York, NY, USA, 10 pages. <https://doi.org/10.1145/3664647.3680812>

1 Introduction

Gait recognition is a technique that identifies pedestrians by analyzing their walking patterns. Unlike other biometric characteristics such as the face and iris, gait can be captured from a distance without pedestrian cooperation, thus attracting increasing attention.

Many advanced appearance-based methods [4, 12, 20, 28] using silhouette sequences as input have obtained successful performance on in-the-lab datasets such as CASIA-B [51] and OU-MVLP [40]. However, the performance of these methods drops dramatically on in-the-wild datasets, *i.e.*, Gait3D [52] and GREW [54]. The primary reason lies in that the scenario of existing in-the-lab datasets differs greatly from in-the-wild ones. In wild scenarios, pedestrians may walk at varying velocities or follow a non-straight routine, and even can be occluded by other pedestrians or objects. These noisy factors are challenging for methods designed according to in-the-lab datasets, resulting in performance degradation.

To address the aforementioned issue, we first compare silhouette sequences between CASIA-B [51] and Gait3D [52] datasets. As shown in Figure 1 (a), multiple and evenly distributed gait circles can be clearly observed from in-the-lab sequences (see pedestrian #1). Thus, appropriate local temporal receptive field can facilitate the model in learning the pattern of a complete gait circle. While in wild scenarios, (see pedestrian #2) such ideal temporal segments are no longer available, since the variations of pace and walking directions have a great influence on the appearance. Therefore, a global temporal receptive field is necessary for aligning gait patterns.

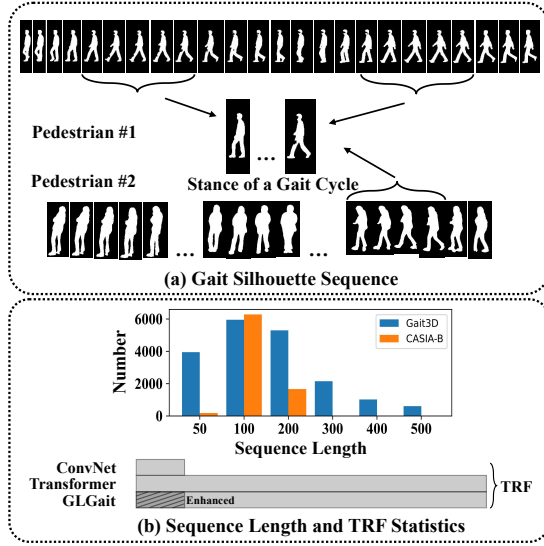


Figure 1: Comparison of local and global temporal receptive field. (a) Gait cycles are evenly distributed in laboratory scenarios (Pedestrian #1), thus proper-sized local receptive field can capture a complete cycle. While in the wild (Pedestrian #2) the distribution is sparse and random, which implies a larger receptive field is necessary. Corresponding sequences are sampled from CASIA-B [51] and Gait3D [52], respectively. (b) Sequence length and TRF statistics in CASIA-B and Gait3D, where TRF is the temporal receptive field.

Recently, some methods [10, 11, 46] have been proposed to address the issue of gait recognition in the wild. These methods are mainly centered around Convolutional Neural Networks (ConvNets). Compared with methods designed according to in-the-lab datasets, they often incorporate more convolutional operations to exhibit a larger receptive field. Given that gait silhouettes are typically quite small, such as 64×64 pixels, the spatial receptive field of these methods is already sufficient. However, the temporal receptive field obtained through convolutional operations is significantly insufficient. As shown in Figure 1 (b), the temporal receptive field usually can only cover around 50 silhouettes in a sequence, which is quite limited in contrast to typical frame number of in-the-wild gait sequences. The limited local temporal receptive field struggles to capture adequate information about pedestrian body shape changes, thus a global temporal receptive field is essential.

Some works [2] use visual transformer block [7] to obtain a global temporal receptive field. However, directly replacing convolution blocks with transformer blocks cannot necessarily enhance a local temporal receptive field. Considering that a transformer block usually applies multi-head self-attention [44] (MHSA) to obtain a global receptive field, adding MHSA before temporal convolution operation in ConvNets is a possible resolution to obtain a global-local temporal receptive field. However, due to using the output of ConvNets as input to MHSA, dimension explosion occurs in token size with large channels in ConvNets, such as 512, resulting in high memory consumption and computation cost. To address the issue, we propose Pseudo Global Temporal Self-Attention (PGTA). Compared with MHSA, PGTA reduces complexity in two aspects. First,

considering the receptive field issue in the temporal dimension, we separate the spatial dimension, only calculating the patch size from the temporal dimension. Secondly, we separate the patch size from tokens in PGTA inspired by [33], obtaining a pseudo temporal receptive field of each element in tokens. With the same temporal convolution kernel size and patch size, these pseudo global temporal receptive fields are naturally aggregated to a truly global one. We name the combination of PGTA and temporal convolution operation as Global-Local Temporal Module (GLTM).

Based on GLTM, we design a Global-Local Temporal Receptive Field Network, named GLGait. The backbone of GLGait consists of a vision encoder and Global-Local 3D (GL-3D) Blocks. In the vision encoder, GLGait encodes a preliminary pedestrian representation. For GL-3D block, in the temporal dimension, GLTM is used to effectively obtain a global-local temporal receptive field. While in the spatial dimension, we use 2D convolution operations, the reason is straightforward: the spatial receptive field is already sufficient by convolution operations.

Furthermore, inspired by center loss [17, 48], we also propose a simple yet effective loss function, named Center-Augmented Triplet Loss (CTL) to assist in model training as a component in GLGait. Based on conventional triplet loss [18], CTL additionally considers the class center as a positive sample for each input. This operation has two advantages: reducing the intra-class distance and expanding the positive samples in the training stage.

The main contributions are summarized as follows:

- 1) We design a Global-Local Temporal Receptive Field Network (GLGait) to obtain a global-local temporal receptive field for gait recognition in the wild.
- 2) We propose Pseudo Global Temporal Self-Attention (PGTA) to reduce the high memory and computation complexity of multi-head self-attention [44] (MHSA).
- 3) We propose a Center-Augmented Triplet Loss (CTL) to assist in model training. CTL can reduce the intra-class distance and expand the positive samples in the training stage.
- 4) Extensive experiments demonstrate that our approach obtains the state-of-the-art performance on in-the-wild datasets, *i.e.*, Gait3D [52] and GREW [54].

2 Related Works

2.1 Model-based Gait Recognition

Model-based methods [1, 13, 25–27, 35, 41, 42, 49] consider the physical structure of the human body and utilize pose information as input, such as 2D skeletons, 3D joints, and point clouds. For instance, PoseGait [27] utilizes the human body pose information to extract temporal-spatial features and employs ConvNets to extract high-level temporal-spatial features. GaitGraph [42] proposes a pose estimator to extract pose features and adopts graph convolutional neural networks [39] for gait recognition. GPgait [13] uses a unified pose representation as input. Then a part-aware graph convolutional network is proposed to enable efficient graph partition and local-global spatial feature extraction. LidarGait [38] leverages LiDAR to generate gait point clouds for gait recognition. Model-based methods are robust in some scenarios, such as clothes changed [5, 37]. However, pose information is not easy to calculate, thus these methods may be difficult to apply in a new scenario.

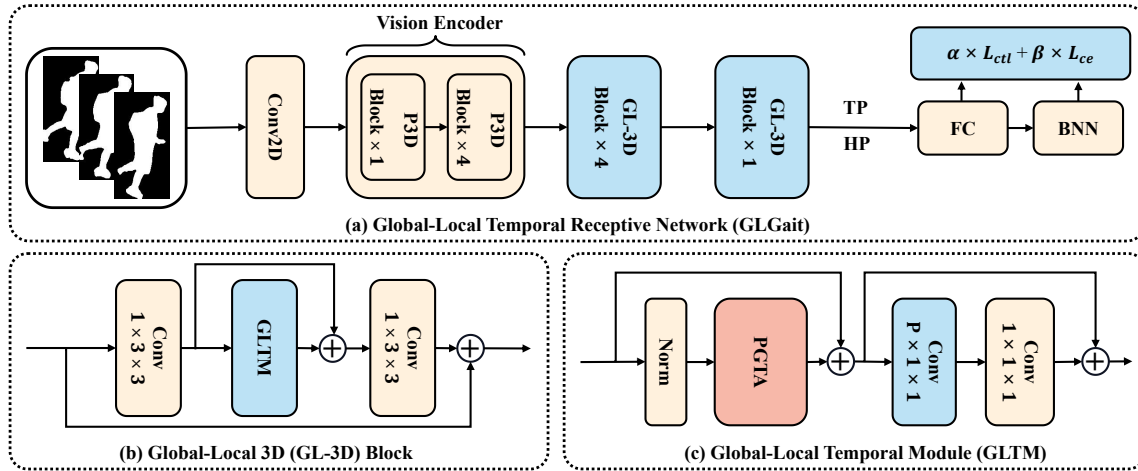


Figure 2: Pipeline of the proposed GLGait. The backbone mainly consists of the vision encoder and GL-3D blocks. Specifically, we use Pseudo Global Temporal Self-Attention (PGTA) to extract global temporal information and a temporal convolution operation to enhance the local temporal information extraction in Global-Local Temporal Module (GLTM). TP denotes the Temporal Max Pooling operation, HP is the Horizontal Pooling operation [11, 14], FC is the separate fully connected layers [4], and BNN is BNNeck [32]. The final loss function is composed of a center-augmented triplet loss (CTL) and a cross-entropy loss.

2.2 Appearance-based Gait Recognition

Appearance-based methods are employed to learn the body appearance without achieving explicit structures. Most methods [3, 4, 8–10, 12, 19, 23, 28, 45, 46, 50] use silhouette sequences as inputs and use deep neural networks to extract feature [16, 22, 36, 43]. Then, by comparing similarities with other silhouette sequences, the recognition is implemented. Some methods [47, 53] also utilize semantic parsing of pedestrians as the input, obtaining satisfactory performance.

Previous works [4, 6, 12, 28] focus on in-the-lab scenarios, obtaining successful performance. However, with the recent development of in-the-wild datasets, *i.e.*, Gait3D [52] and GREW [54], these methods are facing new challenges. To employ precise gait recognition in wild scenarios, some methods are proposed. GaitGCI [9] utilizes counterfactual intervention learning to eliminate the impact of confounder, focusing on the discriminative and interpretable regions effectively. DyGait [46] focuses on the extraction of dynamic features and proposes a dynamic augmentation module to learn part features automatically. Fan et al. [11] proposes a simple yet effective ResNet-like [16] framework, which is referred as GaitBase. Based on GaitBase, DGaitV2 [10] obtains higher accuracy by increasing the number of stacked blocks.

Compared to pose information, appearance cues are relatively easy to obtain in a new scenario, exhibiting broader adaptability. However, appearance information is susceptible to the influence of pedestrian appearance, exhibiting low robustness in certain specific scenarios such as clothes change [5, 37]. Our GLGait belongs to the appearance-based category, using gait silhouette sequences as input and establishing a global-local temporal receptive field.

2.3 Gait Transformers

Vision transformer [7] has achieved successful performance in many fields, such as classification [7], objective detection [29], and semantic segmentation [21]. Some works introduce transformer blocks into the gait recognition framework. TransGait [24] proposes

a set transformer model with a temporal aggregation operation for obtaining set-level spatio-temporal features. SwinGait [10] utilizes convolutional blocks to extract silhouette feature and feed it to swinformer [30, 31] blocks. However, the former cannot enhance the local temporal receptive field, while the latter only obtains a window-global temporal receptive field. Differently, our GLGait employs Global-Local Temporal Module (GLTM) to both maintain global-local temporal receptive fields.

3 Method

In this section, we first introduce the pipeline of GLGait. Then, we detail the vision encoder, Global-Local 3D (GL-3D) block, and center-augmented triplet loss (CTL), respectively. Finally, we explain the optimization.

3.1 Pipeline

The pipeline of the proposed GLGait is shown in Figure 2 (a). A simple 2D convolution operation first initializes the silhouette sequences. Then we utilize the vision encoder to obtain a preliminary representation. After that, GL-3D blocks are used to extract both spatial information and global-local temporal information. Temporal Max Pooling operation (TP) and Horizontal Pooling operation [11, 14] are employed to aggregate the features. Finally, a combined loss function consisting of center-augmented triplet loss and cross-entropy loss is used to supervise the learning process.

3.2 Vision Encoder

Since gait silhouette is binary, containing limited information [10], we use a vision encoder to encode a preliminary pedestrian representation. Specifically, we use the conventional Pseudo 3D (P3D) blocks [16, 36] as the components. P3D block uses two 2D convolutions in the spatial dimension and a 1D convolution in the temporal dimension. Using $\mathbf{x}_{in} \in \mathbb{R}^{C \times T \times H \times W}$ as input, where C is the channels, T is frame number, H and W are the silhouette height

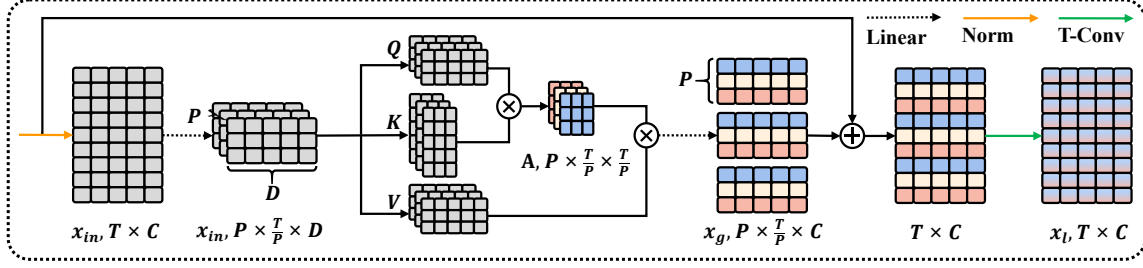


Figure 3: Pseudo Global Temporal Self-Attention (PGTA) with a temporal convolution operation (T-Conv).

and width, respectively. The process can be formulated as

$$\mathbf{x}_1 = \mathcal{R}(C_{2d}(\mathbf{x}_{in})), \quad (1)$$

$$\mathbf{x}_2 = C_{1d}(\mathbf{x}_1), \quad (2)$$

$$\mathbf{x}_3 = C_{2d}(\mathcal{R}(\mathbf{x}_1 + \mathbf{x}_2)), \quad (3)$$

$$\mathbf{x}_{out} = \mathcal{R}(\mathbf{x}_{in} + \mathbf{x}_3), \quad (4)$$

where $\mathbf{x}_{out} \in \mathbb{R}^{C \times T \times H \times W}$ is the output, $C_{1d}(\cdot)$ is the temporal convolution operation, $C_{2d}(\cdot)$ is the spatial convolution operation, \mathcal{R} is the ReLU activation function.

3.3 GL-3D Block

Operation. As shown in Figure 2 (b), GL-3D block consists of two 2D convolutions for spatial information and a Global-Local Temporal Modul (GLTM) for the temporal feature. Specifically, GLTM mainly contains Pseudo Global Temporal Self-Attention (PGTA) and temporal convolution operation as shown in Figure 2 (c). Different from normal multi-head self-attention [44] (MHSA), PGTA places its focus on the temporal dimension, reducing the memory and computation complexity in two aspects. 1) PGTA separates the spatial dimension from the patch size, which means it is only 1D rather than 3D. 2) PGTA separates the patch size from the token inspired by [33]. We exhibit the structure of PGTA in Figure 3, where we only consider one head for simplicity.

Given $\mathbf{x}_{in} \in \mathbb{R}^{L \times T \times C}$ as input, where L is $H \times W$, the formula of PGTA is as follows:

$$\text{Reshaping } \mathbf{x}_{in}, \quad \mathbb{R}^{L \times T \times C} \rightarrow \mathbb{R}^{L \times P \times \frac{T}{P} \times C} \quad (5)$$

$$[\mathbf{q}_i, \mathbf{k}_i, \mathbf{v}_i] = \mathbf{x}_{in} \mathbf{U}_{qkv}^i, \quad \mathbf{U}_{qkv}^i \in \mathbb{R}^{C \times 3D} \quad (6)$$

$$\mathbf{A}_i = \text{softmax}(\mathbf{q}_i \mathbf{k}_i^T / \sqrt{D}), \quad \mathbf{A}_i \in \mathbb{R}^{L \times P \times \frac{T}{P} \times \frac{T}{P}} \quad (7)$$

$$\mathbf{x}_i = \mathbf{A}_i \mathbf{v}_i, \quad \mathbf{x}_i \in \mathbb{R}^{L \times P \times \frac{T}{P} \times D} \quad (8)$$

$$\mathbf{x}_g = [\mathbf{x}_1; \mathbf{x}_2; \dots; \mathbf{x}_k] \mathbf{U}_{msa}, \quad \mathbf{U}_{msa} \in \mathbb{R}^{k \cdot D \times C} \quad (9)$$

$$\text{Reshaping } \mathbf{x}_g, \quad \mathbb{R}^{L \times P \times \frac{T}{P} \times C} \rightarrow \mathbb{R}^{L \times T \times C} \quad (10)$$

where $i \in \{1, 2, \dots, k\}$, k is the number of multi-heads in PGTA, P is patch size, \mathbf{A} is attention matrix, \mathbf{U}_{qkv} and \mathbf{U}_{msa} are parameter matrices in PGTA. After PGTA, a temporal convolution operation is used to enhance the local temporal receptive field. Inspired by [15], we also add skip connections and 1D convolution operation with the kernel size of one as linear layer after PGTA to obtain a sub-update for each element in tokens. The process is formulated as

$$\mathbf{x}_l = \mathcal{R}(C_{1d}(\mathbf{x}_g + \mathbf{x}_{in})), \quad \mathbf{x}_l \in \mathbb{R}^{L \times T \times D_{mid}} \quad (11)$$

$$\mathbf{x}_{out} = \mathbf{x}_l \mathbf{U}_{mlp} + \mathbf{x}_g, \quad \mathbf{U}_{mlp} \in \mathbb{R}^{D_{mid} \times C} \quad (12)$$

where $\mathbf{x}_{out} \in \mathbb{R}^{L \times T \times C}$ is the output of GLTM, \mathcal{R} and $C_{1d}(\cdot)$ are same as operations in Equation (1) and Equation (2), D_{mid} is the channels of hidden layer, \mathbf{U}_{mlp} is parameter matrix.

Discussion. In this subsection, we undertake a memory and computation complexity analysis of PGTA compared with a normal Spatio-Temporal MHSA [2, 44]. Specifically, we consider two kinds of D in Equation (6). One is that D is the same as the token size. Another is that D is a scalar less than C . The input is $\mathbf{x}_{in} \in \mathbb{R}^{L \times T \times C}$. Given token size $P \times C$, we observe that the token size does not affect the computation complexity in Equation (6) and Equation (9) as follows,

$$C_{com} = O\left(\frac{LT}{P}PCD\right) \quad (13)$$

$$= O(LTCD). \quad (14)$$

Therefore, we only consider the computation complexity in Equation (7) and Equation (8). The formula of complexity in MHSA is as

$$C_{mem}^M = O(PCD), \quad (15)$$

$$C_{com}^M = O(N^2D), \quad (16)$$

where N is $\frac{LT}{P}$, C_{mem}^M is the memory complexity in MHSA, and C_{com}^M is the computation complexity in MHSA. The formula of complexity in PGTA is as

$$C_{mem}^P = O(CD), \quad (17)$$

$$C_{com}^P = O(LP \frac{T^2}{P^2}D) \quad (18)$$

$$= O(LTND), \quad (19)$$

where N is $\frac{T}{P}$, C_{mem}^P is the memory complexity in PGTA, and C_{com}^P is the computation complexity in PGTA.

First, we assume that D is the same as the token size, which means information loss does not occur. For MHSA, given the token size $P_l \times P_t \times C$, where P_l is spatial dimension size and P_t is temporal dimension size, the memory complexity is $O(P_l^2 P_t^2 C^2)$ and the computation complexity is $O(\frac{L^2 T^2}{P_l P_t} C)$. For PGTA, given the token size $P_t \times C$, the memory complexity is $O(P_t C^2)$ and the computation complexity is $O(L T^2 C)$. Compared with MHSA, PGTA reduces the memory complexity significantly, from $O(P_l^2 P_t^2 C^2)$ to $O(P_t C^2)$. For computation complexity, the decrease lies in L and $P_l \times P_t$. Specifically, we set P_t as 3 and P_l as 4 in our experiments. Given L as 16×12 in GL-3D block, L is 16 times than $P_l \times P_t$, meaning PGTA reduces the computation complexity to 1/16 of MHSA.

Secondly, we assume that D is a scalar less than C , which means information loss occurs, especially when the token size is large.

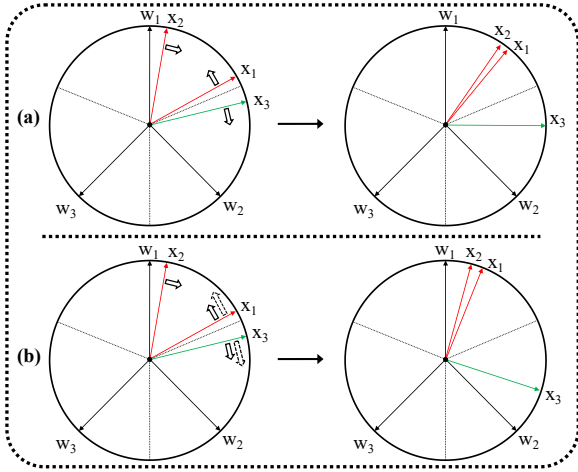


Figure 4: Comparison of triplet loss [18] (a) and proposed center-augmented triplet loss (b). w_i is class center in BN-Neck [32], x_i is sample feature, dashed lines in the circle are class boundaries, \Rightarrow is the gradient of the feature.

For MHSA, given the token size $P_l \times P_t \times C$, the memory complexity is $O(P_l P_t C D)$ and the computation complexity is $O(\frac{L^2 T^2}{P_l^2 P_t^2} D)$. For PGTA, given the token size $P_t \times C$, the memory complexity is $O(CD)$ and the computation complexity is $O(L \frac{T^2}{P_t} D)$. PGTA also reduces the memory complexity significantly, from $O(P_l P_t C D)$ to $O(CD)$. For computation complexity, the decrease lies in L and $P_l^2 \times P_t$. Following the same set above, PGTA reduces the computation complexity to a quarter of MHSA. Furthermore, MHSA loses much information. Assuming the feature dimension is a measure, the information loss of PGTA is only $O(C - D)$. For MHSA, the information loss even reaches $O(P_l P_t C - D)$.

Finally, considering the memory complexity, we set D as a scalar in all our experiments.

3.4 Center-Augmented Triplet Loss

Operation. In contrast to the conventional triplet loss [18], the center-augmented triplet loss (CTL) additionally incorporates class centers as positive instances for each sample, the formulation is given as

$$\mathcal{L}_{ctl}(\mathbf{x}) = \sum_{i=1}^{Q+1} \sum_{j=1}^N \max(\mathcal{D}(\mathbf{x}, \mathbf{x}_i^q) - \mathcal{D}(\mathbf{x}, \mathbf{x}_j^n) + m, 0), \quad (20)$$

$$\mathcal{L}_{ctl} = \frac{1}{B} \sum_{k=1}^B \mathcal{L}_{ctl}(\mathbf{x}_k), \quad (21)$$

where $\mathbf{x} \in \mathbb{R}^C$ is input, \mathbf{x}_i^q is the i -th positive sample of \mathbf{x} , \mathbf{x}_j^n is the j -th negative sample of \mathbf{x} , $\mathcal{D}(\cdot, \cdot)$ is distance function, m is margin, Q is the number of positive samples, N is the number of negative samples, B is the batch size ($B = Q + N + 1$). Specifically, \mathbf{x}_{Q+1}^q is the class center of \mathbf{x} , and Euclidean distance is used in $\mathcal{D}(\cdot, \cdot)$.

Discussion. In this subsection, we discuss the mechanism of center-augmented triplet loss (CTL). Apart from the common effects of triplet loss [18], CTL has two advantages.

First, CTL reduces intra-class distance. As illustrated in Figure 4 (a), for sample $\mathbf{x}_1, \mathbf{x}_2$ is a positive sample, and \mathbf{x}_3 is a negative one. When the distance between $(\mathbf{x}_1, \mathbf{x}_2)$ exceeds that of $(\mathbf{x}_1, \mathbf{x}_3)$, the triplet loss computes the corresponding gradient represented as solid-line arrows, encouraging $(\mathbf{x}_1, \mathbf{x}_2)$ to move closer, and $(\mathbf{x}_1, \mathbf{x}_3)$ to move apart. However, as \mathbf{x}_2 moves closer to \mathbf{x}_1 , it keeps away the class center \mathbf{w}_1 , thus increasing the intra-class distance. Conversely, as shown in Figure 4 (b), by treating \mathbf{w}_1 as a positive sample for \mathbf{x}_1 and \mathbf{w}_3 as one for \mathbf{x}_3 , CTL calculates the respective gradients depicted as dashed-line arrows, driving \mathbf{x}_1 towards \mathbf{w}_1 and \mathbf{x}_3 towards \mathbf{w}_3 . Due to the superposition of gradients from $(\mathbf{x}_1, \mathbf{x}_2)$ and $(\mathbf{x}_1, \mathbf{w}_1)$, \mathbf{x}_1 moves closer to \mathbf{w}_1 , indirectly preventing \mathbf{x}_2 away from the class center \mathbf{w}_1 , thus reducing the intra-class distance.

Secondly, CTL can directly increase the number of positive samples without expanding the batch size. In gait datasets such as Gait3D [52], many pedestrian silhouette sequences are limited in quantity, which means a lack of positive samples in a batch. CTL utilizes class centers as positive samples, adding computational complexity to the loss function without affecting the backbone computations of the model in the training stage and model inference in the test stage, presenting a good cost-effective trade-off.

3.5 Optimization

In the training stage of GLGait, a combined loss function consisting of center-augmented triplet loss (\mathcal{L}_{ctl}) and cross-entropy loss (\mathcal{L}_{ce}) is calculated to supervise the learning process,

$$\mathcal{L} = \alpha \mathcal{L}_{ctl} + \beta \mathcal{L}_{ce}, \quad (22)$$

where α and β are hyper-parameters to balance the contributions to the total loss \mathcal{L} .

4 Experiments

In this section, we first introduce the datasets and implementation details. Then, we compare our proposed GLGait with the latest gait recognition methods and analyze the results. Finally, extensive ablation experiments prove the effectiveness of each component in GLGait.

4.1 Datasets and Implementation Details

The dataset information and implementation details in our experiments are as follows.

Gait3D [52] is a large scale gait dataset. Within a supermarket, 39 cameras capture 1,090 hours of videos with 1,920×1,080 resolution and 25 FPS. Through processing, a total of 4,000 subjects, 25,309 sequences, and 3,279,239 frame images are extracted. 3,000 subjects are compiled as the training set, while the remaining 1,000 subjects form the test set. For the testing phase, the probe comprises one sequence from each subject, and the gallery consists of the rest sequences.

GREW [54] is one of the largest gait datasets in the wild, including Silhouettes, GEIs, and 2D/3D human poses data types. The raw videos are collected from 882 cameras in large public areas. 7,533 video clips are used, containing nearly 3,500 hours of 1,920×1,080 streams. It has 26,345 subjects and 128,671 sequences, divided into two parts with 20,000 and 6,000 subjects as training set and test set,

Table 1: Comparisons of Rank-1, 5 and 10 accuracies, mean Average Precision (%), and Parameter size (M) on Gait3D [52] and GREW [54] datasets.

Backbone Components	Method	Source	Gait3D			GREW			Params
			Rank-1	Rank-5	mAP	Rank-1	Rank-5	Rank-10	
Convolution	GaitSet [4]	AAAI 2019	36.7	58.3	30.0	46.3	63.6	70.3	2.56
	GaitPart [12]	CVPR 2020	28.2	47.6	21.6	44.0	60.7	67.3	1.46
	GaitGL [28]	ICCV 2021	29.7	48.5	22.3	47.3	63.6	69.3	2.49
	SMPLGait [52]	CVPR 2022	42.9	63.9	35.2	-	-	-	-
	DyGait [46]	ICCV 2023	66.3	80.8	56.4	71.4	83.2	86.8	-
	HSTL [45]	ICCV 2023	61.3	76.3	55.5	62.7	76.6	81.3	4.05
	GaitGCI [9]	CVPR 2023	50.3	68.5	39.5	68.5	80.8	84.9	-
	GaitBase [11]	CVPR 2023	64.3	79.6	55.5	59.1	74.5	78.9	4.90
Convolution	DGaitV2-2D-B [10]	Arxiv 2023	64.5	81.7	56.5	62.3	76.4	81.5	2.35
	DGaitV2-2D-L [10]		67.8	83.9	59.7	69.7	82.4	86.7	9.33
	DGaitV2-P3D-B [10]		70.8	85.7	62.9	72.6	84.5	87.9	2.79
	DGaitV2-P3D-L [10]		74.2	86.9	67.1	78.3	88.5	91.4	11.12
	DGaitV2-P3D-H [10]		75.0	-	-	81.0	-	-	44.43
	DGaitV2-3D-B [10]		71.0	85.0	62.3	73.1	84.9	88.4	6.92
	DGaitV2-3D-L [10]		74.1	87.0	66.5	79.0	88.9	91.6	27.62
	DGaitV2-3D-H [10]		75.8	-	-	81.6	-	-	110.44
Convolution + Transformer	SwinGait-3D [10]	Arxiv 2023	75.0	86.7	67.2	79.3	88.9	91.8	13.1
	GLGait-B	Ours	73.9	86.3	65.9	75.4	86.3	89.6	3.58
	GLGait-L		77.6	88.4	69.6	80.0	89.4	92.2	14.28
	GLGait-H		77.7	88.9	70.6	82.8	91.1	93.5	57.04

respectively. Each subject in the test set has four sequences, two for probe and two for gallery.

Implementation Details. Our experiments are implemented using PyTorch [34]. We design the network capacity referring to the baselines [10, 11] as shown in Table 2. In Equation 22, α and β are both set to 1. The kernel size of all convolution operations is 3. In Equation 8, P is set to 3, and D is the same as C in Stage-1. In Equation 11, D_{mid} is the same as C in all stages. For parameters, we only consider the backbone without FC [4] and BNN [32] layers for all experiments. Similar to DGaitV2 [10], we also partition the model size into three segments: GLGait-Base (GLGait-B), GLGait-Large (GLGait-L), and GLGait-Huge (GLGait-H) to exhibit an appropriate compromise between accuracy and cost. They share identical architectures, except for the variation in the number of channels at each stage, which are (32, 64, 128, 256), (64, 128, 256, 512), and (128, 256, 512, 1024), respectively. During training, the input size of silhouettes is 64×44 , and silhouettes are ordered in a sequence with a length of 30. The optimizer is the Stochastic Gradient Descent (SGD). The weight decay is 0.0005 and the momentum is 0.9. We adjust the learning rate, batch size, and the number of iterations to fit different dataset scales. 1) On Gait3D, we train the model for 120k iterations with a batch size of 32×4 (32 pedestrians, each containing 4 sequences). The learning rate starts at 0.1 and is subsequently decreased by a factor of 0.1 at iterations (40k, 80k, 100k). 2) On GREW, the model is trained for 180k iterations with a batch size of 32×4 . The learning rate starts at 0.05 and is subsequently decreased by a factor of 0.2 at iterations (60k, 120k, 150k).

Specifically, we train the models in GaitBase [11] and DGaitV2 [10] by ourselves. As shown in Table 1, the results on the left side of the parentheses represent our results, while the results inside the parentheses originate from the original paper [10, 11].

4.2 Performance Comparison

We compare our approach with other recent appearance-based methods using silhouette sequence as input on in-the-wild datasets as shown in Table 1. Specifically, the input to SMPLGait [52] is exclusively comprised of the silhouette. These methods can be divided into two categories based on the network backbone components: one category backbone predominantly consists of convolutional operations, while another category backbone is constituted of both convolutional operations and transformers.

For the first category, the receptive field plays an essential role. For the spatial receptive field, as illustrated in Table 1, despite DGaitV2-2D-B [10] having half the parameters of GaitBase [11], its spatial receptive field substantially exceeds that of GaitBase, ultimately surpassing GaitBase in accuracy on Gait3D [52] and GREW [54] by 0.2% and 3.2%, respectively. The second consideration is the temporal receptive field. Under equivalent spatial receptive field conditions, DGaitV2-P3D-B outperforms DGaitV2-2D-B by 6.3% and 10.3% Rank-1 accuracy on Gait3D and GREW with only 0.44 MegaBytes parameters increase; a similar trend is observed with DGaitV2-P3D-L and DGaitV2-2D-L. However, no matter for DGaitV2-P3D or DGaitV2-3D, in comparison to sequences extending hundreds of silhouettes, their temporal receptive fields are significantly insufficient, merely extracting limited local temporal information.

For the second category, we consider that a global-local temporal receptive field shall be important. As depicted in Figure 1 (a), gait exhibits a certain cyclical pattern, and this cycle represents a local silhouette sequence within gait sequences. SwinGait-3D [10] utilizes a 3D residual block to encode a preliminary pedestrian representation, which is then fed into a 3D Swinformer [30, 31]

Table 2: Network backbone of the GLGait.

Layer Name	Output Size	Structure $[k \times k \times k, c] \times b$
Conv2D	$(T, C, 64, 44)$	$[1 \times 3 \times 3, C] \times 1$
Stage-1 Vision Encoder	$(T, C, 64, 44)$	$\begin{bmatrix} 1 \times 3 \times 3, C \\ 3 \times 1 \times 1, C \\ 1 \times 3 \times 3, C \end{bmatrix} \times 1$
Stage-2 Vision Encoder	$(T, 2C, 32, 22)$	$\begin{bmatrix} 1 \times 3 \times 3, 2C \\ 3 \times 1 \times 1, 2C \\ 1 \times 3 \times 3, 2C \end{bmatrix} \times 4$
Stage-3 GL-3D Block	$(T, 4C, 16, 11)$	$\begin{bmatrix} 1 \times 3 \times 3, 4C \\ GLTM, 4C \\ 1 \times 3 \times 3, 4C \end{bmatrix} \times 4$
Stage-4 GL-3D Block	$(T, 8C, 16, 11)$	$\begin{bmatrix} 1 \times 3 \times 3, 8C \\ GLTM, 8C \\ 1 \times 3 \times 3, 8C \end{bmatrix} \times 1$

Table 3: Extended experiment of sequence length on Gait3D with Rank-1 accuracy (%).

Method	Sequence Length					
	1-100	101-200	201-300	301-400	401-500	1-500
DGaitV2-P3D-L	68.8	84.1	75.3	83.0	75.0	74.2
GLGait-L	71.7	84.1	76.4	88.1	85.7	76.6

block, achieving a window-global temporal receptive field. However, within these blocks, SwinGait-3D cannot obtain a true global one. In contrast, GLGait utilizes GLTM to exhibit a global-local temporal receptive field, thereby more effectively learning the cyclical motions of gait. With similar parameter counts, GLGait surpasses SwinGait-3D in Rank-1 accuracy both on Gait3D and GREW by 1.6% and 0.4%.

Moreover, we conduct an extended experiment to further explore the performance of GLGait across varying sequence lengths. The results are shown in Table 3, where the length distribution is illustrated in Figure 1 (b). GLGait-L outperforms DGaitV2-P3D-L 5.1% and 10.7% Rank-1 accuracy at lengths 301 to 400 and 401 to 500, respectively. This demonstrates that GLGait is effective in long sequences. Besides, we also observe that GLGait improves 2.9% Rank-1 accuracy at lengths 1 to 100, indicating that GLGait is even effective in short sequences rather than only in long sequences.

Finally, with the incorporation of CTL, GLGait-H achieves state-of-the-art performance on both Gait3D and GREW, obtaining Rank-1 accuracy of 77.7% and 82.8%, respectively.

Effectiveness of Center-Augmented Triplet Loss. To verify the effectiveness of CTL, we conduct ablation experiments on DGaitV2-P3D [10] and GLGait. As shown in Table 4, CTL improves both DGaitV2-P3D and GLGait compared with conventional triplet loss [18] on Gait3D [52] and GREW [54], demonstrating its generalizability and effectiveness. Meanwhile, we also compare CTL with center loss [48] (CL) and triplet center loss [17] (TCL) as shown in Table 5. CTL outperforms them in GLGait-B and GLGait-L. The reason lies in that CL and TCL only focus on the connection between samples and class centers, ignoring the pair of samples to samples. In contrast, CTL considers the pair of both samples to samples and samples to class centers, reducing intra-class distance

Table 4: Performance gain from applying CTL on Gait3D [52] and GREW [54] with Rank-1 accuracy (%).

Method	Gait3D	GREW
DGaitV2-P3D-B [10]	70.8 \rightarrow 72.1	72.6 \rightarrow 74.3
DGaitV2-P3D-L [10]	74.2 \rightarrow 75.4	78.3 \rightarrow 79.6
GLGait-B	73.3 \rightarrow 73.9	74.2 \rightarrow 75.4
GLGait-L	76.6 \rightarrow 77.6	79.7 \rightarrow 80.0

Table 5: Compared center-augmented triplet loss (CTL) with other loss function on Gait3D [52] with Rank-1 accuracy (%), where TL is triplet loss [18], CL is center loss [48], TCL is triplet center loss [17].

Method	TL	CL	TCL	CTL	Rank-1
GLGait-B	✓	-	-	-	73.3
	-	✓	-	-	72.8
	-	-	✓	-	73.3
	-	-	-	✓	73.9
GLGait-L	✓	-	-	-	76.6
	-	✓	-	-	76.1
	-	-	✓	-	76.2
	-	-	-	✓	77.6

and expanding positive samples. CTL can seamlessly substitute conventional triplet loss [18], and we substitute it with CTL in subsequent experiments.

4.3 Ablation Experiments

We exhibit ablation experiments in GLGait to prove the effectiveness of each component.

Vision Encoder Size. To explore an appropriate vision encoder size, we conduct ablation studies within a controlled network, where the number of channels and blocks in per stage are fixed. Specifically, we employed the P3D block [16, 36] as the component of the vision encoder. As shown in Table 6, the model demonstrates optimal performance when S-1 and S-2 are both employed as the vision encoder, at which point the vision encoder is capable of learning an effective preliminary representation of pedestrians. Utilizing only S-1 as the vision encoder fails to obtain a satisfactory preliminary pedestrian representation, diminishing the model’s learning efficiency within the GL-3D block. Conversely, incorporating S-1, S-2, and S-3 as the vision encoder does not afford additional space for the GL-3D block, impeding the model’s ability to learn an effective global temporal receptive field and consequently degrading model performance. Finally, we employ S-1 and S-2 as the vision encoder.

Vision Encoder Component. We also exhibit the component ablation experiments on the vision encoder in Table 7. When employing P3D block [16, 36] as the component, GLGait obtains a better result with fewer parameters compared with 3D block [16, 36]. The possible reason lies in that our GL-3D block also separates the spatial and temporal dimensions, which is similar to P3D block. Maintaining such a similar structure assists in model training. Meanwhile, for 2D block [16], although it has fewer parameters, it is unable to process temporal information, which is essential in pedestrian representation, thus the performance significantly drops out.



Figure 5: Silhouette score in Temporal Max Pooling phase, where the sequence contains 474 silhouettes from Gait3D.

Table 6: Ablation study of vision encoder size on Gait3D [52] with Rank-1 accuracy (%) and Params (M), where S-i is Stage-i, and checkmark (✓) indicates that the stage is utilized as a part of the vision encoder.

Method	S-1	S-2	S-3	S-4	Rank-1	Params
GLGait-B	✓	-	-	-	73.5	3.76
	✓	✓	-	-	73.9	3.58
	✓	✓	✓	-	72.6	3.12
	✓	✓	✓	✓	72.6	3.12
GLGait-L	✓	-	-	-	76.6	15.00
	✓	✓	-	-	77.6	14.28
	✓	✓	✓	-	76.4	12.44
	✓	✓	✓	✓	76.4	12.44

Table 7: Ablation study of vision encoder components on Gait3D [52] with Rank-1 accuracy (%), and Params (M).

Method	Components	Rank-1	Params
GLGait-B	2D block [16]	72.4	3.52
	3D block [16, 36]	73.1	4.12
	P3D block [16, 36]	73.9	3.58
GLGait-L	2D block [16]	75.2	14.07
	3D block [16, 36]	76.4	16.43
	P3D block [16, 36]	77.6	14.28

Finally, we select P3D block as the component in the vision encoder to obtain a good accuracy and cost trade-off.

Effectiveness of PGTA. To verify the effectiveness of Pseudo Global Temporal Self-Attention (PGTA), we compare it with other multi-head self-attention [44] methods, containing Spatio-Temporal MHSA [2], Factorised self-attention [2] on temporal dimension, and MobileViT [33] self-attention. Specifically, we set patch size to 3×4 . The results are shown in Table 8. PGTA reduces half of the parameters compared with Spatio-Temporal MHSA and Factorised self-attention. Meanwhile, we observe that the Rank-1 accuracy of Spatio-Temporal MHSA and Factorised self-attention greatly drops out. The possible reason is that a large information loss occurs between the 3,072 token size (patch size \times channels) and 256 channels. Compared with MobileViT self-attention, PGTA improves 1.9% Rank-1 accuracy with fewer FLOPs. Due to the issue of the receptive field lying in the temporal dimension, PGTA only focuses on the temporal dimension and separates the spatial dimension from tokens, thus effectively establishing a good solution.

Effectiveness of Temporal Convolution after PGTA. To verify the effectiveness of temporal convolution after PGTA, we compare it with a normal linear operation. As shown in Table 9, employing temporal convolution improves GLGait-B 1.6% and GLGait-L 1.1% Rank-1 accuracy than a normal linear operation with few parameters increase. Temporal convolution enhances the local receptive field, assisting the model in learning the motion process of gait. Besides, temporal convolution can also aggregate pseudo

Table 8: Ablation study of memory and computation complexity in self-attention [44] on Gait3D [52] with Rank-1 accuracy (%), Params (M), and FLOPs (G).

Method	Module	R-1	Params	FLOPs
GLGait-B	Spatio-Temporal MHSA [2]	68.2	7.93	0.93
	Factorised self-attention [2]	70.6	7.93	0.92
	MobileViT self-attention [33]	72.0	3.58	0.94
	PGTA	73.9	3.58	0.87

Table 9: Ablation study of temporal convolution after PGTA on Gait3D [52] with Rank-1 accuracy (%), and Params (M).

Method	Temporal Convolution	Rank-1	Params
GLGait-B	-	72.3	3.32
	✓	73.9	3.58
GLGait-L	-	76.5	13.23
	✓	77.6	14.28

global temporal receptive fields generated by PGTA to a true holistic temporal receptive field. Its effectiveness is well demonstrated.

4.4 Visualization

To verify the effectiveness of GLGait in long sequences, we conduct visualization as illustrated in Figure 5, where the score is model attention in temporal max pooling phase for each silhouette. GLGait can detect dynamic sub-sequences and give them high scores; for static sub-sequences, it selects representative silhouettes to give high scores and assigns low scores to the rest. This demonstrates that GLGait can align various gait patterns in long sequences, thus validating the effectiveness of global-local temporal receptive field.

5 Conclusion

In this paper, to address the issue of temporal receptive field for gait recognition in the wild, we add the multi-head self-attention (MHSA) before temporal convolution operation in Convolutional Neural Networks (ConvNets), designing a Global-Local Temporal Receptive Field Network (GLGait) to obtain a global-local temporal receptive field. Due to the dimension explosion in MHSA, we propose a Pseudo Global Temporal Self-Attention (PGTA) to reduce the memory and computation complexity. Furthermore, a Center-Augmented Triplet Loss (CTL) is proposed to reduce the intra-class distance and expand the positive samples, seamlessly substituting conventional triplet loss. GLGait can effectively recognize pedestrians with limited memory and computation complexity in wild scenarios, thus this work can be applied to widespread surveillance gait recognition systems. Extensive experiments have been conducted on Gait3D and GREW. The results demonstrate that our approach outperforms state-of-the-art methods on in-the-wild datasets.

Acknowledgments

This work was supported by the Key Program of National Natural Science Foundation of China (Grant No. U20B2069) and research funding from Kuaishou Technology.

References

- [1] Weizhi An, Shiqi Yu, Yasushi Makihara, Xinhui Wu, Chi Xu, Yang Yu, Rijun Liao, and Yasushi Yagi. 2020. Performance evaluation of model-based gait on multi-view very large population database with pose sequences. *IEEE Transactions on Biometrics, Behavior, and Identity Science* 2, 4 (2020), 421–430.
- [2] Anurag Arnab, Mostafa Dehghani, Georg Heigold, Chen Sun, Mario Lucic, and Cordelia Schmid. 2021. Vivit: A video vision transformer. In *IEEE/CVF International Conference on Computer Vision*. 6836–6846.
- [3] Tianrui Chai, Annan Li, Shaoxiong Zhang, Zilong Li, and Yunhong Wang. 2022. Lagrange Motion Analysis and View Embeddings for Improved Gait Recognition. In *IEEE/CVF Conference on Computer Vision and Pattern Recognition*. 20249–20258.
- [4] Hanqing Chao, Yiwei He, Junping Zhang, and Jianfeng Feng. 2019. Gaitset: Regarding Gait as A Set for Cross-view Gait Recognition. In *AAAI Conference on Artificial Intelligence*, Vol. 33. 8126–8133.
- [5] Patrick Connor and Arun Ross. 2018. Biometric recognition by gait: A survey of modalities and features. *Computer Vision and Image Understanding* 167 (2018), 1–27.
- [6] Muqing Deng, Zhuyao Fan, Peng Lin, and Xiaoren Feng. 2024. Human Gait Recognition Based on Frontal-view Sequences Using Gait Dynamics and Deep Learning. *IEEE Transactions on Multimedia* 26 (2024), 117–126.
- [7] Alexey Dosovitskiy, Lucas Beyer, Alexander Kolesnikov, Dirk Weissenborn, Xiuhua Zhai, Thomas Unterthiner, Mostafa Dehghani, Matthias Minderer, Georg Heigold, Sylvain Gelly, Jakob Uszkoreit, and Neil Houlsby. 2021. An Image is Worth 16x16 Words: Transformers for Image Recognition at Scale. In *9th International Conference on Learning Representations*.
- [8] Huanzhang Dou, Pengyi Zhang, Wei Su, Yunlong Yu, and Xi Li. 2022. Metagait: Learning to learn an omni sample adaptive representation for gait recognition. In *European Conference on Computer Vision*. 357–374.
- [9] Huanzhang Dou, Pengyi Zhang, Wei Su, Yunlong Yu, Yining Lin, and Xi Li. 2023. GaitGCI: Generative Counterfactual Intervention for Gait Recognition. In *IEEE/CVF Conference on Computer Vision and Pattern Recognition*. 5578–5588.
- [10] Chao Fan, Saihui Hou, Yongzhen Huang, and Shiqi Yu. 2023. Exploring Deep Models for Practical Gait Recognition. *arXiv preprint arXiv:2303.03301* (2023).
- [11] Chao Fan, Junhao Liang, Chuanfu Shen, Saihui Hou, Yongzhen Huang, and Shiqi Yu. 2023. OpenGait: Revisiting Gait Recognition Towards Better Practicality. In *IEEE/CVF Conference on Computer Vision and Pattern Recognition*. 9707–9716.
- [12] Chao Fan, Yunjie Peng, Chunshui Cao, Xu Liu, Saihui Hou, Jiannan Chi, Yongzhen Huang, Qing Li, and Zhiqiang He. 2020. Gaitpart: Temporal Part-based Model for Gait Recognition. In *IEEE/CVF Conference on Computer Vision and Pattern Recognition*. 14225–14233.
- [13] Yang Fu, Shibe Meng, Saihui Hou, Xuecai Hu, and Yongzhen Huang. 2023. GP-Gait: Generalized Pose-based Gait Recognition. In *IEEE/CVF International Conference on Computer Vision*. 19595–19604.
- [14] Yang Fu, Yunchao Wei, Yuqian Zhou, Honghui Shi, Gao Huang, Xinchao Wang, Zhiqiang Yao, and Thomas Huang. 2019. Horizontal Pyramid Matching for Person Re-identification. In *AAAI Conference on Artificial Intelligence*, Vol. 33. 8295–8302.
- [15] Mor Geva, Avi Caciularu, Kevin Ro Wang, and Yoav Goldberg. 2022. Transformer Feed-Forward Layers Build Predictions by Promoting Concepts in the Vocabulary Space. In *Proceedings of the 2022 Conference on Empirical Methods in Natural Language Processing*. 30–45.
- [16] Kaiming He, Xiangyu Zhang, Shaoqing Ren, and Jian Sun. 2016. Deep Residual Learning for Image Recognition. In *IEEE/CVF Conference on Computer Vision and Pattern Recognition*. 770–778.
- [17] Xinwei He, Yang Zhou, Zhichao Zhou, Song Bai, and Xiang Bai. 2018. Triplet-center loss for multi-view 3d object retrieval. In *IEEE/CVF Conference on Computer Vision and Pattern Recognition*. 1945–1954.
- [18] Alexander Hermans, Lucas Beyer, and Bastian Leibe. 2017. In Defense of the Triplet Loss for Person Re-Identification. *arXiv preprint arXiv:1703.07737* (2017).
- [19] Saihui Hou, Chunshui Cao, Xu Liu, and Yongzhen Huang. 2020. Gait lateral network: Learning discriminative and compact representations for gait recognition. In *European conference on computer vision*. 382–398.
- [20] Xiaohu Huang, Duowang Zhu, Hao Wang, Xinggang Wang, Bo Yang, Botao He, Wenyu Liu, and Bin Feng. 2021. Context-sensitive Temporal Feature Learning for Gait Recognition. In *IEEE/CVF International Conference on Computer Vision*. 12909–12918.
- [21] Alexander Kirillov, Eric Mintun, Nikhila Ravi, Hanzi Mao, Chloe Rolland, Laura Gustafson, Tete Xiao, Spencer Whitehead, Alexander C Berg, Wan-Yen Lo, et al. 2023. Segment anything. In *IEEE/CVF International Conference on Computer Vision*. 4015–4026.
- [22] Yann LeCun, Léon Bottou, Yoshua Bengio, and Patrick Haffner. 1998. Gradient-based learning applied to document recognition. *Proc. IEEE* 86, 11 (1998), 2278–2324.
- [23] Aoqi Li, Saihui Hou, Qingyuan Cai, Yang Fu, and Yongzhen Huang. 2024. Gait Recognition with Drones: A Benchmark. *IEEE Transactions on Multimedia* 26 (2024), 3530–3540.
- [24] Guodong Li, Lijun Guo, Rong Zhang, Jiangbo Qian, and Shangce Gao. 2023. Transgait: Multimodal-based gait recognition with set transformer. *Applied Intelligence* 53, 2 (2023), 1535–1547.
- [25] Na Li and Xinbo Zhao. 2023. A Strong and Robust Skeleton-Based Gait Recognition Method with Gait Periodicity Priors. *IEEE Transactions on Multimedia* 25 (2023), 3046–3058.
- [26] Xiang Li, Yasushi Makihara, Chi Xu, Yasushi Yagi, Shiqi Yu, and Mingwu Ren. 2020. End-to-end model-based gait recognition. In *Proceedings of the Asian Conference on Computer Vision*.
- [27] Rijun Liao, Shiqi Yu, Weizhi An, and Yongzhen Huang. 2020. A model-based gait recognition method with body pose and human prior knowledge. *Pattern Recognit* 98:107069 (2020).
- [28] Beibei Lin, Shunli Zhang, and Xin Yu. 2021. Gait Recognition via Effective Global-Local Feature Representation and Local Temporal Aggregation. In *IEEE/CVF International Conference on Computer Vision*. 14648–14656.
- [29] Yaoyao Liu, Bernt Schiele, Andrea Vedaldi, and Christian Rupprecht. 2023. Continual detection transformer for incremental object detection. In *IEEE/CVF Conference on Computer Vision and Pattern Recognition*. 23799–23808.
- [30] Ze Liu, Yutong Lin, Yue Cao, Han Hu, Yixuan Wei, Zheng Zhang, Stephen Lin, and Baining Guo. 2021. Swin transformer: Hierarchical vision transformer using shifted windows. In *IEEE/CVF International Conference on Computer Vision*. 10012–10022.
- [31] Ze Liu, Jia Ning, Yue Cao, Yixuan Wei, Zheng Zhang, Stephen Lin, and Han Hu. 2022. Video swin transformer. In *IEEE/CVF Conference on Computer Vision and Pattern Recognition*. 3202–3211.
- [32] Hao Luo, Youzhi Gu, Xingyu Liao, Shenqi Lai, and Wei Jiang. 2019. Bag of Tricks and A Strong Baseline for Deep Person Re-identification. In *IEEE/CVF Conference on Computer Vision and Pattern Recognition Workshops*.
- [33] Sachin Mehta and Mohammad Rastegari. 2022. MobileViT: Light-weight, General-purpose, and Mobile-friendly Vision Transformer. In *10th International Conference on Learning Representations*.
- [34] Adam Paszke, Sam Gross, Francisco Massa, Adam Lerer, James Bradbury, Gregory Chanan, Trevor Killeen, Zeming Lin, Natalia Gimelshein, Luca Antiga, et al. 2019. Pytorch: An imperative style, high-performance deep learning library. *Advances in Neural Information Processing Systems* 32 (2019).
- [35] Ekkasit Pinyoanuntapong, Ayman Ali, Pu Wang, Minwoo Lee, and Chen Chen. 2023. GaitMixer: skeleton-based gait representation learning via wide-spectrum multi-axial mixer. In *IEEE International Conference on Acoustics, Speech and Signal Processing*. 1–5.
- [36] Zhaofan Qiu, Ting Yao, and Tao Mei. 2017. Learning Spatio-Temporal Representation with Pseudo-3D Residual Networks. In *IEEE/CVF International Conference on Computer Vision*. 5534–5542.
- [37] Sudeep Sarkar, P Jonathon Phillips, Zongyi Liu, Isidro Robledo Vega, Patrick Grother, and Kevin W Bowyer. 2005. The humanoid gait challenge problem: Data sets, performance, and analysis. *IEEE Transactions on Pattern Analysis and Machine Intelligence* 27, 2 (2005), 162–177.
- [38] Chuanfu Shen, Chao Fan, Wei Wu, Rui Wang, George Q Huang, and Shiqi Yu. 2023. Lidargait: Benchmarking 3d gait recognition with point clouds. In *IEEE/CVF Conference on Computer Vision and Pattern Recognition*. 1054–1063.
- [39] Yi-Fan Song, Zhang Zhang, Caifeng Shan, and Liang Wang. 2020. Stronger, faster and more explainable: A graph convolutional baseline for skeleton-based action recognition. In *Proceedings of the 28th ACM International Conference on Multimedia*. 1625–1633.
- [40] Noriko Takemura, Yasushi Makihara, Daigo Muramatsu, Tomio Echigo, and Yasushi Yagi. 2018. Multi-view Large Population Gait Dataset and Its Performance Evaluation for Cross-view Gait Recognition. *IPSI Transactions on Computer Vision and Applications* 10 (2018), 1–14.
- [41] Torben Teepe, Johannes Gilg, Fabian Herzog, Stefan Hörmann, and Gerhard Rigoll. 2022. Towards a Deeper Understanding of Skeleton-based Gait Recognition. In *IEEE/CVF Conference on Computer Vision and Pattern Recognition Workshops*. 1568–1576.
- [42] Torben Teepe, Ali Khan, Johannes Gilg, Fabian Herzog, Stefan Hörmann, and Gerhard Rigoll. 2021. Gaitgraph: Graph convolutional network for skeleton-based gait recognition. In *International Conference on Image Processing*. 2314–2318.
- [43] Du Tran, Lubomir D. Bourdev, Rob Fergus, Lorenzo Torresani, and Manohar Paluri. 2015. Learning Spatiotemporal Features with 3D Convolutional Networks. In *IEEE/CVF International Conference on Computer Vision*. 4489–4497.
- [44] Ashish Vaswani, Noam Shazeer, Niki Parmar, Jakob Uszkoreit, Llion Jones, Aidan N Gomez, Łukasz Kaiser, and Illia Polosukhin. 2017. Attention is all you need. *Advances in Neural Information Processing Systems* 30 (2017).
- [45] Lei Wang, Bo Liu, Fangfang Liang, and Bincheng Wang. 2023. Hierarchical Spatio-Temporal Representation Learning for Gait Recognition. In *IEEE/CVF*

- International Conference on Computer Vision*. 19639–19649.
- [46] Ming Wang, Xianda Guo, Beibei Lin, Tian Yang, Zheng Zhu, Lincheng Li, Shunli Zhang, and Xin Yu. 2023. DyGait: Exploiting Dynamic Representations for High-performance Gait Recognition. In *IEEE/CVF International Conference on Computer Vision*. 13424–13433.
 - [47] Zengbin Wang, Saihui Hou, Man Zhang, Xu Liu, Chunshui Cao, and Yongzhen Huang. 2023. GaitParsing: Human Semantic Parsing for Gait Recognition. *IEEE Transactions on Multimedia* (2023).
 - [48] Yandong Wen, Kaipeng Zhang, Zhifeng Li, and Yu Qiao. 2016. A discriminative feature learning approach for deep face recognition. In *European Conference on Computer Vision*. 499–515.
 - [49] Ke Xu, Xinghao Jiang, and Tanfeng Sun. 2022. Gait recognition based on local graphical skeleton descriptor with pairwise similarity network. *IEEE Transactions on Multimedia* 24 (2022), 3265–3275.
 - [50] Lingxiang Yao, Worapan Kusakunniran, Peng Zhang, Qiang Wu, and Jian Zhang. 2023. Improving disentangled representation learning for gait recognition using group supervision. *IEEE Transactions on Multimedia* 25 (2023), 4187–4198.
 - [51] Shiqi Yu, Daoliang Tan, and Tieniu Tan. 2006. A Framework for Evaluating the Effect of View Angle, Clothing and Carrying Condition on Gait Recognition. In *International Conference on Pattern Recognition*, Vol. 4. IEEE, 441–444.
 - [52] Jinkai Zheng, Xinchun Liu, Wu Liu, Lingxiao He, Chenggang Yan, and Tao Mei. 2022. Gait Recognition in the Wild with Dense 3D Representations and A Benchmark. In *IEEE/CVF Conference on Computer Vision and Pattern Recognition*. 20228–20237.
 - [53] Jinkai Zheng, Xinchun Liu, Shuai Wang, Lihao Wang, Chenggang Yan, and Wu Liu. 2023. Parsing is all you need for accurate gait recognition in the wild. In *Proceedings of the 31st ACM International Conference on Multimedia*. 116–124.
 - [54] Zheng Zhu, Xianda Guo, Tian Yang, Junjie Huang, Jiankang Deng, Guan Huang, Dalong Du, Jiwen Lu, and Jie Zhou. 2021. Gait Recognition in the Wild: A Benchmark. In *IEEE/CVF International Conference on Computer Vision*. 14789–14799.